Gene 529 (2013) 228–237

Contents lists available at ScienceDirect

Gene

journal homepage: www.elsevier.com/locate/gene

Splicing variants of the porcine betaine–homocysteine S-methyltransferase gene: Implications for mammalian metabolism

Radhika Ganu [a], Timothy Garrow [b], Markos Koutmos [c], Laurie Rund [d], Lawrence B. Schook [a,d,*]

[a] Division of Nutritional Sciences, University of Illinois, Urbana, IL 61801, USA
[b] Department of Food Science and Human Nutrition, University of Illinois, Urbana, IL 61801, USA
[c] Department of Biochemistry and Molecular Biology, Uniformed Services University of the Health Sciences, Bethesda, MD 20814, USA
[d] Department of Animal Sciences, University of Illinois, Urbana, IL 61801, USA

ARTICLE INFO

Article history:
Accepted 30 July 2013
Available online 13 August 2013

Keywords:
Betaine
Homocysteine
Splice variant
Bisulfite sequencing

ABSTRACT

Betaine–homocysteine S-methyltransferase (BHMT) activity is only detected in the liver of rodents, but in both the liver and kidney cortex of humans and pigs; therefore, the pig was chosen as a model to define the spatial and temporal expression of BHMT during development. During fetal development, a total of ten splice variants of *bhmt* were expressed at varying levels across a wide range of porcine tissues. Two variants contained an identical ORF that encoded a C-terminal truncated form of BHMT (tBHMT). The *bhmt* transcripts were expressed at significant levels in the liver and kidney from day 45 of gestation (G45) onward. The transcripts encoding tBHMT represented 5–13% of the total *bhmt* transcripts in G30 fetus, G45 liver, and adult liver and kidney cortex. The dominant structural feature of wild type BHMT is an $(\beta\alpha)_8$ barrel, however, a modeled structure of tBHMT suggests that this protein would assume a horseshoe fold and lack methyltransferase activity. Low BHMT activity was detected in the G30 fetus, and slightly increased levels of activity were observed in the liver from G45 and G90 fetuses. The *bhmt* promoter contained three key CpG sites, and methylation of these sites was significantly higher in adult lung compared to adult liver. The data reported herein suggest that genomic DNA methylation and variation of the 5′ and 3′ UTRs of *bhmt* transcripts are key regulators for the level of *BHMT* transcription and translation.

1. Introduction

Elevated levels of homocysteine (Hcy) in blood, hyperhomocysteinemia, has been associated with an increased risk for vascular disease and thrombosis (Refsum et al., 1998) and neural tube defects and adverse pregnancy outcomes, including spina bifida and placental abruptions (Ananth et al., 2007; Eskes, 1998; Hague, 2003; James et al., 1999; Mills et al., 1995; Steegers-Theunissen et al., 1991). Hcy resides at a metabolic branch point; it can proceed through the transsulfuration pathway to participate in cysteine biosynthesis or it can be remethylated to form methionine, the amino acid from which it was derived. Hcy remethylation is important to sustain adequate Met availability for the synthesis of S-adenosylmethionine, the required methyl donor for hundreds of S-adenosylmethionine-dependent methyltransferase enzymes found in mammals (Petrossian and Clarke, 2011). There are nutritional conditions and genetic factors known to reduce Hcy remethylation and cause hyperhomocysteinemia, presumably increasing disease risk.

There are three cytosolic enzymes in mammals that remethylate Hcy; methionine synthase (EC 2.1.1.13), betaine–homocysteine S-methyltransferase (BHMT, EC 2.1.1.5), and the recently characterized BHMT-2 (EC 2.1.1.5) (Szegedi et al., 2008). Methionine synthase is a cobalamin-dependent enzyme that uses 5-methyltetrahydrofolate as the methyl donor. BHMT uses betaine, whereas BHMT-2 uses S-methylmethionine, as its methyl donor. Methionine synthase is a low abundance protein whose activity can be detected in nearly every mammalian tissue. However, BHMT and BHMT-2 activities are largely restricted to the liver, and in some species, kidney or pancreas, but the detection of these enzymes can be hampered by their low turnover numbers, which are about a 1000-fold less than methionine synthase (Garrow, 1996; Millian and Garrow, 1998; Szegedi et al., 2008).

Much is known about the structure of BHMT since the crystal structures of the human (Evans et al., 2002) and rat (Gonzalez et al., 2004) enzymes have been solved. In brief, the primary sequence of BHMT is encoded by ~400 amino acids and its quaternary structure is a tetramer composed of a dimer of dimers. The first three-quarters of the ORF encode a $(\beta/\alpha)_8$ barrel that contains all but one of the known residues that form the active site, including residues Cys217, Cys299 and

Abbreviations: BHMT, betaine–homocysteine S-methyltransferase (protein); *bhmt*, betaine–homocysteine S-methyltransferase (gene); tBHMT, truncated form of BHMT; UTR, untranslated region; Hcy, homocysteine; SV, splice variant.

* Corresponding author at: Department of Animal Sciences, University of Illinois, 1201 West Gregory Avenue, Urbana, IL, USA. Tel.: +1 217 265 5326; fax: +1 217 244 5617.
E-mail address: schook@illinois.edu (L.B. Schook).

0378-1119/$ – see front matter © 2013 Elsevier B.V. All rights reserved.
http://dx.doi.org/10.1016/j.gene.2013.07.103

Cys300, which are required for binding the enzyme's catalytic zinc, as well as Gln159, an invariant residue in this family of enzymes required for Hcy binding. The C-terminal region, defined as the last quarter of the ORF, encodes structures required for oligomerization (Evans et al., 2002; Gonzalez et al., 2004).

It is unclear why mammals have three cytosolic enzymes that methylate Hcy, and little is known regarding their relative contributions to methionine biosynthesis and how their contributions might change with physiological state or diet, or how their expression in various tissues might change throughout development. With respect to BHMT, one other known physiological function is to regulate betaine concentrations in liver and kidney (Delgado-Reyes and Garrow, 2005). Relative to the low abundance of methionine synthase, it is intriguing that BHMT represents up to 1% or more of the total soluble protein in adult liver (Garrow, 1996). Is it possible that BHMT has a moonlighting function(s) yet to be discovered? An alternative function could explain why BHMT has not evolved to be a more efficient catalyst, or why mammalian liver expresses so much BHMT since its activity and cellular location is redundant to methionine synthase.

The pig has been established as a good animal model to study several human diseases including diabetes, Alzheimer's disease, and cancer (Tumbleson and Schook, 1996). Since pigs express BHMT in the same adult organs as humans (Sunden et al., 1997), we chose to use them as a model to identify and explore the spatial and temporal expression of *bhmt* transcripts arising throughout development, and gain clues regarding a potential moonlighting function(s) for its gene product(s). Variation in heteronuclear RNA splicing can increase protein diversity and more than three quarters of mammalian genes are alternatively spliced (Johnson et al., 2003). This report is the first to describe and quantify *bhmt* splice variants during pig development, including two variants that when translated would encode a truncated protein predicted to have no methyltransferase activity. We also report that promoter methylation and length variation of the *bhmt* 5′ and 3′ UTRs probably have important roles in regulating the expression level of BHMT in different tissues.

2. Materials and methods

2.1. BHMT enzyme assay

The BHMT assay was performed using the method described by Garrow (Garrow, 1996) with the following modifications. The betaine concentration used was 250 μM and the incubation was performed at 37 °C for 30 min for adult liver, fetal (G45 and G90) liver and adult kidney cortex, and 2 h for G30 fetus, and G45 and G90 kidney, lungs, heart and brain and adult lungs, heart and brain tissues. The incubation time for liver samples was reduced since BHMT activity is highest in liver. Samples from three animals were analyzed separately for each tissue. The negative control (no enzyme added) in the experiment was used as blank and the values were normalized to the amount of protein present in the tissue using Bradford method thereby determining the specific activity.

2.2. RNA extraction and cDNA preparation

Tissues were obtained from adult (sexually mature) and fetal gestation days 30, 45 and 90 from three Yorkshire pigs. The tissues at these developmental stages (whole fetus was used for analyzing gestation day 30) were liver, kidney cortex, kidney medulla, lungs, heart, and brain. Total RNA was isolated from frozen tissues using the RNeasy Mini Kit (Qiagen, Valencia, CA). Reverse transcription was carried out using random primers and the Bioline cDNA synthesis kit (Taunton, MA).

2.3. Cloning and sequencing BHMT splice variants (SV)

Based on the exonic regions of the porcine *bhmt* gene, cDNAs that together encode the complete ORF of BHMT were amplified using the following three primer sets (Table 1); 1-F/1-R, 2-F/2-R, and 3-F/3-R (Ganu et al., 2011). Then, the 5′ and 3′ untranslated regions of *bhmt* transcripts from various tissues were amplified using total RNA and the FirstChoice™ RNA ligase-mediated (RLM)-RACE kit (Ambion, Austin, TX). This procedure used primers supplied with the kit and the nested gene-specific primers listed in Table 1. The 5′ UTRs from all tissues were obtained using the B1-5r-outer/5′-RACE-outer and B1-5r-inner/5′ RACE inner primer sets. The 3′ UTR from liver was obtained using the B1-3r-outer/3′-RACE-outer and B1-3r-inner/3′ RACE-inner primer sets (Ganu et al., 2011). The 3′ UTRs from adult kidney medulla, lung, brain and heart were isolated following two rounds of amplification with the following primer sets; B1-Sv-3r-outer/3′-RACE-outer and B1-Sv-3r-inner/3′-RACE-inner. These products were cloned into pCRTOPO2.1 vector and sequenced. The sequences of bhmt splice variants were submitted to NCBI genbank. SV1 (HQ130333) was previously reported (Ganu et al., 2011) but the accession numbers of the others are SV2 (JX988430), SV3(JX988431), SV4(JX988432), SV5(JX988433), SV6(JX988434), SV7(JX988435), SV8(JX988436), SV9(JX988437) and SV10(JX988438). The cDNAs and deduced amino acid sequences were

Table 1
List of primers used for amplifying.

Primer name	Primer sequence	Tm	Experiment
B1-Sv-3r-outer	CCTTGAAAGCATCTGGGAAG	60	RLM-RACE
B1-Sv-3r-inner	GCTCATGAAAGAAGGCTTGC	60	RLM-RACE
B1-5r-outer	TCCGTCTCCAATCACAACCT	60	RLM-RACE
3′RACE-outer	Supplied with kit	60	RLM-RACE
3′RACE-inner	Supplied with kit	60	RLM-RACE
5′RACE-outer	Supplied with kit	60	RLM-RACE
5′RACE-inner	Supplied with kit	60	RLM-RACE
BHMT-exon6-7-F	GGTTCATCGACCTGCCAGAA	–	Real-time RT-PCR
BHMT-exon6-7-R	GAATGTCCCATCTGGTTGCAA	–	Real-time RT-PCR
BHMT-exon6-8-F	GCAAACAGTGAAGCTCATGAAAGA	–	Real-time RT-PCR
BHMT-exon6-8-R	CATCCGGCTTTGACATGGA	–	Real-time RT-PCR
BHMT-exon6-8-probe	AGGCCATACAACCC	–	Real-time RT-PCR
Mp-1f	GTTTTTTATATTTTTATAATTAGAGGA	55.3	Bisulfite sequencing
Mp-1r	AACTCCCTACCTACAAAATCCTC	55.3	Bisulfite sequencing
Mp-2f	GATTTTGTAGGTAGGGAGTT	55.3	Bisulfite sequencing
Mp-2r	AAACCCAATAAAAACCCTACAACTT	55.3	Bisulfite sequencing
Mp-3f	TTTTTTTGGTTTTTTTGTTTTTAAT	52.8	Bisulfite sequencing
Mp-3r	AACAAATAACAACCTACTTATTTTT	52.8	Bisulfite sequencing
Mp-4f	GGGGTTATATAGTTTTAGGGGG	55.9	Bisulfite sequencing
Mp-4r	ACCAAAAAAATAAATCTACAAAAACC	55.9	Bisulfite sequencing

analyzed using the Biology Workbench (http://workbench.sdsc.edu/). The mRNA secondary structures and free energy values were predicted using the MFOLD software program (version 3.2; http://www.bioinfo.rpi.edu/applications/mfold)(Zuker, 2003). Poly AH software (http://www.softberry.ru/berry.phtml) was used to detect poly A signal sites. Potential miRNA sites were identified using miRwalk (http://www.umm.uni-heidelberg.de/apps/zmf/mirwalk/predictedmirnagene.html). MiRWalk also compares additional miRNA predicting algorithms such as miRanda, miRDB, PITA, RNAhybrid, RNA22. TargetScan algorithm was used to predict miRNA sites (http://www.targetscan.org/). The putative tBHMT protein was modeled using Phyre software (www.sbg.bio.ic.ac.uk/~phyre/), and visual depictions were generated using the PyMOL Molecular Visualization System (DeLano Scientific LLC, Palo Alto, CA). The pdb code of the structure used as a 3D template for the homology modeling is 1LT8.

2.4. Real-time RT-PCR of porcine BHMT SVs

SVs were quantified by RT-PCR using the SYBR Green PCR Mastermix. Total mRNA was treated with RNase-free DNAse (Qiagen, Valencia, CA) to eliminate genomic contamination. Reverse transcription was then performed using the OmniscriptKit (Qiagen, Valencia, CA) (Chen et al., 2006). The primers used to quantify the *bhmt* transcrips (Table 1) were designed using Primer Express software (Applied Biosystems, Foster City, CA). The total amount of *bhmt* mRNA (all splice variants) in a given tissue was determined using the qBHMT-f/qBHMT-r primer set (Ganu et al., 2011). Transcripts sharing the exon 6–exon 7 junction (SV1, SV2, SV4, SV5, SV7, SV8, SV9 and SV10) were measured using a primer located at the 3′ end of exon 6 (BHMT-exon6-7-F) and another primer annealing with the 5′ end of exon 7 (BHMT-exon6-7-R). In order to accurately quantify the truncated splice variants (SV3 and SV6), a Taqman 5′ nuclease assay (Applied Biosystems, Foster City, CA) using the BHMT-exon6-8-F/BHMT-exon6-8-R primer set was performed. The probe (BHMT-exon6-8-probe) was designed to anneal to the specific exon 6–exon 8 junction found only in SV3 and SV6. Using these data, the percentage of transcripts encoding wild type (WT) BHMT (SV1, SV2, SV4, SV5, SV5, SV7, SV8 and SV9) and tBHMT (SV3 and SV6) were determined. Three replicates were performed for each sample. Each reaction contained 100 ng of cDNA. The negative controls (minus template or reverse transcriptase) were run in triplicate. Data was normalized using 18S ribosomal RNA as an internal control and to the amount of genomic DNA/tissue/sample (Chen et al., 2006). The parameters used for qPCR were 50 °C for 2 min followed by 95 °C for 10 min, 40 cycles with 95 °C for 15 s, 60 °C for 1 min, final cycle of 95 °C for 15 s, 60 °C for 15 s and 95 °C for 15 s. Splice variants were cloned into pCR2.1-TOPO (Invitrogen, Carlsbad, CA), verified by sequencing and used for the construction of a standard curve. The qRT-PCR assay was performed using the ABI 7900HT fast real-time PCR system (Applied Biosystems, Foster City, CA). Statistical analyses were performed using ANOVA ($p < 0.01$).

2.5. Bisulfite sequencing of bhmt CpG island

Genomic DNA was isolated from the liver and lung of three adult pigs (sexually mature; 7 months) and three G90 embryos. The EpiTect Bisulfite Kit (Qiagen, Valencia, CA) was used for bisulfite conversion of genomic DNA. The primers given in Table 1 were used to amplify the *bhmt* CpG island. The PCR program used for primer Mp-1, Mp-2, and Mp-4 was 94 °C for 5 min, 94 °C for 30 s, 52–56 °C for 30 s, 72 °C for 1 min and 72 °C for 10 min. The PCR program used for primer Mp-3 was 94 °C for 5 min, 94 °C for 30 s, 52.8 °C for 3 min, 72 °C for 1 min and 72 °C for 10 min. A total of 35 cycles were performed all PCR reactions. The PCR products were then cloned into pCR2.1-TOPO (Invitrogen, Carlsbad, CA), sequenced using ABI Big Dye, and the percentage of methylated (CpG) sites was determined. A total of 24 clones were sequenced using a minimum of 4 clones from each animal. For G90 liver primer set Mp-3, a total of 23 clones were sequenced with a minimum of 6 clones from each animal.

3. Results

3.1. BHMT enzymatic activity during development

BHMT activity was greater in adult liver (123 U/mg) followed by adult kidney cortex (28 U/mg). Adult kidney medulla and brain had low activity (5 U/mg), whereas adult lung had no detectable activity. The amount of BHMT activity in whole G30 fetus was ~3 U/mg, and fetal liver at G45 and G90 had 5 and 11 U/mg, respectively (Fig. 1). There was no detectable BHMT activity in kidney, lungs, heart and brain tissues of G45 and G90 fetuses.

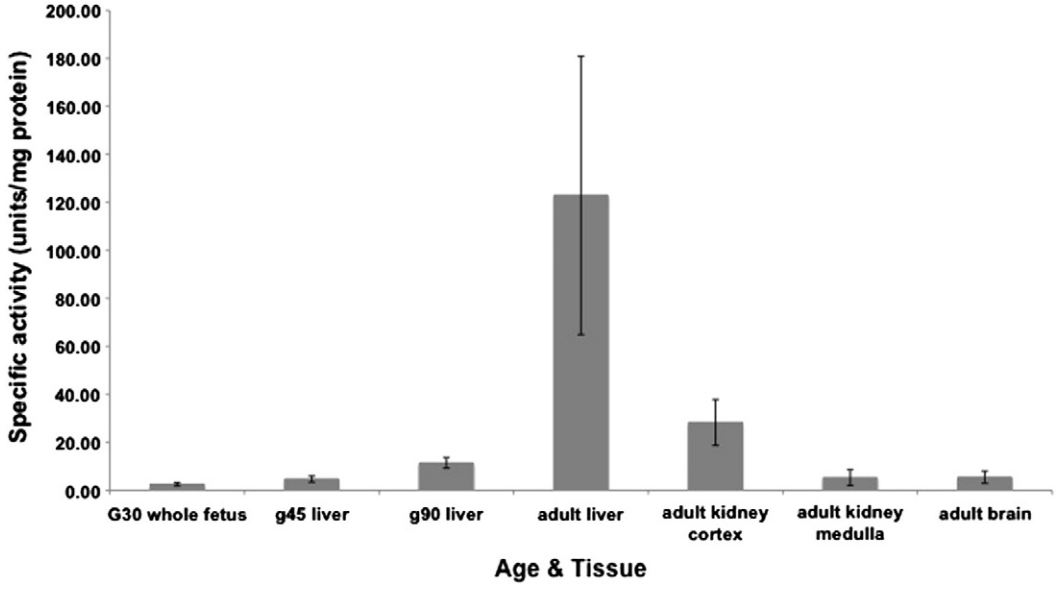

Fig. 1. BHMT enzyme activity during development in different tissues. The gray bars represent the specific activity of BHMT methyltransferase activity in units/mg protein. Total protein content was measured using Bradford assay. The error bars represent standard deviation observed from three different animal samples.

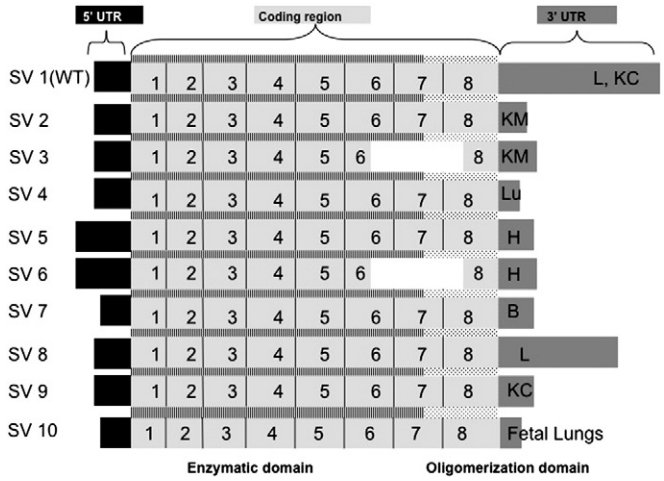

Fig. 2. Splice variants (SV) of *bhmt* gene. The black boxes represent the 5′ UTR, light gray boxes numbered 1–8 represent the exon 1–8 and the dark gray boxes represent the 3′ UTR. In addition to coding sequence, exon 1 and exon 8 include the 5′ UTR and 3′ UTR, respectively. The black vertical lines depict region coding for the enzymatic region of BHMT protein and black dotted region depicts the oligomerization domain. The letters represent L (liver), KC (kidney cortex), KM (kidney medulla), Lu (lungs), H (heart), B (brain).

3.2. Analysis of bhmt splice variants and deduced amino acid sequences

Analysis of total RNA obtained from adult liver, kidney cortex, kidney medulla, lungs, heart and brain revealed the presence of ten *bhmt* splice variants (Fig. 2). SV1 has been previously reported in (Ganu et al., 2011). The entire ORF encoded by the *bhmt* gene is composed of 8 exons (1224 bp) and encodes a protein of 407 amino acids (45 kD) (Ganu et al., 2011). Seven of the nine variants encoded this protein, which is consistent with the enzymes purified from rat (Gonzalez et al., 2004), pig (Sunden et al., 1997) and human liver (Garrow, 1996). Interestingly, two splice variants (SV3 and SV6) encode an identical ORF that is missing the latter half of exon 6, all of exon 7, and the beginning of exon 8 compared to the other SV. If translated, these variants would encode a tBHMT protein composed of 255 residues (28 kD).

3.3. 5′UTR and 3′UTR analyses

The varying lengths of the 5′ and 3′ UTRs of the SVs are depicted in Fig. 2, and their precise lengths as well as the length of the coding regions for individual SVs are given in Table 2. The 5′ UTRs were predicted to have secondary structures with free energies ranging from −19.5 (SV1; liver) to −56.5 to −59.4 kcal/mol (SV5/6; heart). Using miRNA predicting softwares (miRWalk, miRanda, miRDB and Targetscan), a potential miRNA (mmu-miR-686) was found in a mouse BHMT 3′ UTR (NM_016668), and this potential miRNA is conserved in the 3′ UTR of porcine (SV1 and SV8) that are detected in the liver and kidney cortex.

Table 2
Length of UTRs and coding region of BHMT splice variants.

Splice variant	5′ UTR (nucleotide)	Coding region (nucleotides)	3′ UTR (nucleotide)
1	77	1224	1142
2	77	1224	79
3	77	768	161
4	77	1224	74
5	162	1224	79
6	162	768	161
7	74	1224	79
8	77	1224	927
9	77	1224	79
10	74	1224	74

3.4. Tissue-specific expression analyses of porcine BHMT splice variants

To compare the expression levels of the SV in different tissues, the primer pairs listed in Table 1 were used for real-time PCR analysis. The total expression of *bhmt* transcripts is provided in Table 3. Consistent with activity measurements, adult liver expressed the highest levels of *bhmt* mRNA followed by the kidney cortex. The kidney medulla and lungs expressed lower ($p < 0.01$) transcript levels, and adult heart and brain had the lowest levels. In G45 fetal tissues, the transcript expression pattern followed the same trend, with the liver and kidney expressing high levels with comparatively lower levels observed in lungs, heart and brain. In G90 fetal tissues, high levels of *bhmt* mRNA were observed in the porcine liver and kidney, but no transcripts were detected in the lungs, heart and brain. The relative ratio of transcripts with exon 7 (SV1, 2, 4, 5, 7, 8 and 9), which encode the wild type BHMT, relative to those without exon 7 (SV3, 6), which encode tBHMT, is given in Table 4. Since adult liver expresses high levels of *bhmt* mRNA, the expression level of the isoforms that encode tBHMT were biologically significant. In some tissues, the total of SV3/6 and SV1/2/4/5/7/8/9/10 exceeded the number of total *bhmt* transcripts (detected using primers in exon4) indicating that there could be additional SV that have not been detected by our screening methods. The total *bhmt* transcript expression in a given organ was strongly correlated to that organ's level of BHMT activity ($R^2 = 0.68$), however, because all of the variants that can code for an active enzyme only differed in their 5′ and 3′ UTRs, it is not possible to determine if a given transcript(s) more reliably predicts activity within a given tissue.

3.5. Modeled structure of tBHMT

Two splice variants (SV3 and SV6) isolated from the kidney medulla and heart, respectively, were found to contain an identical ORF that was significantly shorter than the ORF encoded by the other SVs, including the primary isoform found in liver (SV1), which defines the wild type protein. Based on its primary sequence, if efficiently translated and stable, tBHMT would lack methyltransferase activity since it lacks key residues required for catalysis, including Cys299 and Cys300, both of which are required for zinc binding, and in turn is required for Hcy binding and therefore catalysis (Breksa and Garrow, 2002; Evans et al., 2002). Furthermore, tBHMT also lacks sequences that encode the C-terminal region of wild type BHMT that are required for oligomerization, suggesting that tBHMT would be present as a monomeric protein. The translated tBHMT peptide was modeled based on hBHMT

Table 3
Expression of total bhmt transcripts using qRT-PCR.

Age	Tissue	Average bhmt transcripts/100 ng cDNA	Standard deviation
g30	G30fetus	40,509	18,030
g45	Liver	127,199	56,613
	Kidney medulla	Not detectable	–
	Kidney cortex	136,922	64,710
	Lungs	27,546	12,260
	Heart	14,583	6491
	Brain	1620	721
g90	Liver	401,852	178,854
	Kidney medulla	Not detectable	–
	Kidney cortex	203,357	90,509
	Lungs	4861	2164
	Heart	Not detectable	–
	Brain	Not detectable	–
Adult	Liver	1,675,464	745,705
	Kidney medulla	288,750	128,515
	Kidney cortex	1,453,473	646,903
	Lungs	116,667	51,925
	Heart	76,157	33,896
	Brain	15,799	7032

Table 4
Relative ratio of presence of splice variants.

	G30 (whole fetus)	G45	G90	Adult
Liver SV (6–7)	90%	94%	86%	88%
Liver SV (6–8)	10%	6%	13%*	12%
Kidney cortex SV (6–7)	-	86%	100%	92%
Kidney cortex SV (6–8)	–	13%	ND	8%
Kidney medulla SV (6–7)	–	ND	ND	100%
Kidney medulla SV (6–8)	–	ND	ND	ND
Lungs SV (6–7)	–	ND	ND	100%
Lungs SV (6–8)	–	ND	ND	ND
Heart SV (6–7)	–	ND	ND	24%
Heart SV (6–8)	–	ND	ND	ND

ND = splice variants below detection levels.
6–7 = splice variants sharing exon 6–7 junction.
6–8 = splice variants sharing exon 6–8 junction.
* = Average of three replicates from one animal.

(PDB 1LT8) using the Phyre server (Kelley and Sternberg, 2009) while molecular figures were created with PyMOL (Schrodinger, 2010) (Fig. 3). The model suggests that tBHMT is missing the N-terminal α-helix, β-strand and αB helix, as well as the C-terminal α-helix and β-strand of the wild type enzyme, and that tBHMT assumes a horseshoe rather than a barrel fold.

3.6. Analysis of methylation status of CpG islands

A CpG island (865 bp with 64.9% GC content) was detected in the porcine *bhmt* gene. This island is located 100 bp upstream of the translational start site and contains exon 1 and part of intron 1. The methylation status of adult and G90 fetal liver and lungs was studied in order to understand if methylation could be a factor contributing to the spatial and temporal regulation of *bhmt* gene since mRNA and enzyme activity are abundant in liver and kidney cortex. The CpG island was cloned using primers that amplified four overlapping regions (Fig. 4).

The overall methylation of the CpG island was 5.7% for adult liver and 19.1% for adult lungs. The key sites of methylation were −10, −67 and −69, which are part of the consensus T-Ag and M2F1 transcription factor binding sites. In adult liver, none of these sites were methylated except in one out of 24 clones (CpG located −69; 3% methylation). The part of CpG island contained within the promoter region in adult liver was not methylated. In the case of adult lungs the CpG sites located at −10, −67 and −69 were 13.26%, 39.32% and 33.18% methylated, respectively. Thus, the level of methylation

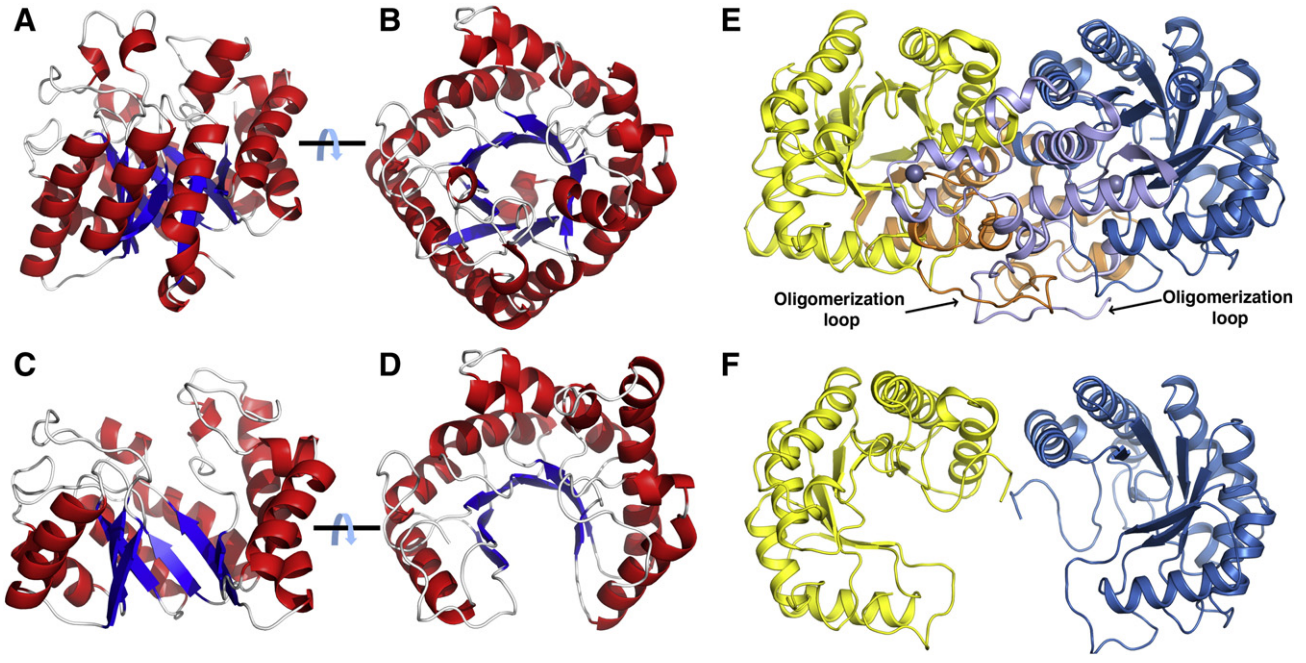

Fig. 3. Structure of hBHMT (PDB 1LT8) and modeled structure of tBHMT. (A) and (B) show the structure of wild type human BHMT (barrel only), and (C) and (D) show the Phyre-generated model of the truncated form of porcine BHMT (tBHMT). (E) Dimer of hBHMT where the two monomers are shown in cartoon and displayed in blue and yellow. Zn atoms are shown in gray spheres. The regions highlighted in orange and light blue are equivalent to the regions missing in the porcine BHMT SV1 and SV6 variants. These regions are involved in extensive dimerization interactions. (F) Two tBHMT monomers were superimposed to the two momoners comprising the hBHMT dimer. It is clear that tBHMT lacks important residues that would promote dimerization in a manner similar to that of the full-length enzyme.

is correlated to the expression of *bhmt* gene in adult liver and lungs. Transcription of the *bhmt* gene in liver was 40-fold higher than in adult lungs. The overall methylation of the CpG island was 10.25% for G90 liver and 15.15% for G90 lungs. The part of CpG island contained within the promoter region of fetal liver was 13.8% methylated but was 20.83% in fetal lungs. No specific methylation pattern was observed for the fetal pigs indicating that methylation could be a factor for regulation only in adulthood.

4. Discussion

A previous study reported that BHMT mRNA (via Northern analysis), activity, and immunodetectable protein could only be detected in the liver and kidney cortex of adult pigs (Ganu et al., 2011; Sunden et al., 1997). Using adult pig tissues, this study confirms that most of the BHMT activity in pigs is sequestered to these adult organs. However, due to the increased sensitivity of PCR, we have characterized a total of ten *bhmt* SVs that were expressed in a variety of adult and fetal porcine tissues. The SVs differed in the length of their 5′ and 3′ UTRs, and two variants encoded the same novel ORF, that if effectively translated, would encode a C-terminal truncated form of BHMT. Furthermore, it would not be possible for the tBHMT protein to have methyltransferase activity since missing residues are required for binding its catalytic zinc.

The UTRs and coding regions of the different SV are depicted in Fig. 2, and their precise lengths are given in Table 2. Sequence analyses predicted that the free energy for the secondary structure of the leader sequence encoded by the dominant variant in liver (SV1), which is where BHMT mRNA and activity are most abundant, is only −19.5 kcal/mol. In contrast, the free energies for the secondary structures predicted for the leader sequences found in heart (SV5 and SV6), where dramatically lower levels of BHMT mRNA and activity were observed, were greater than −50 kcal/mol. Previous studies have shown that when the

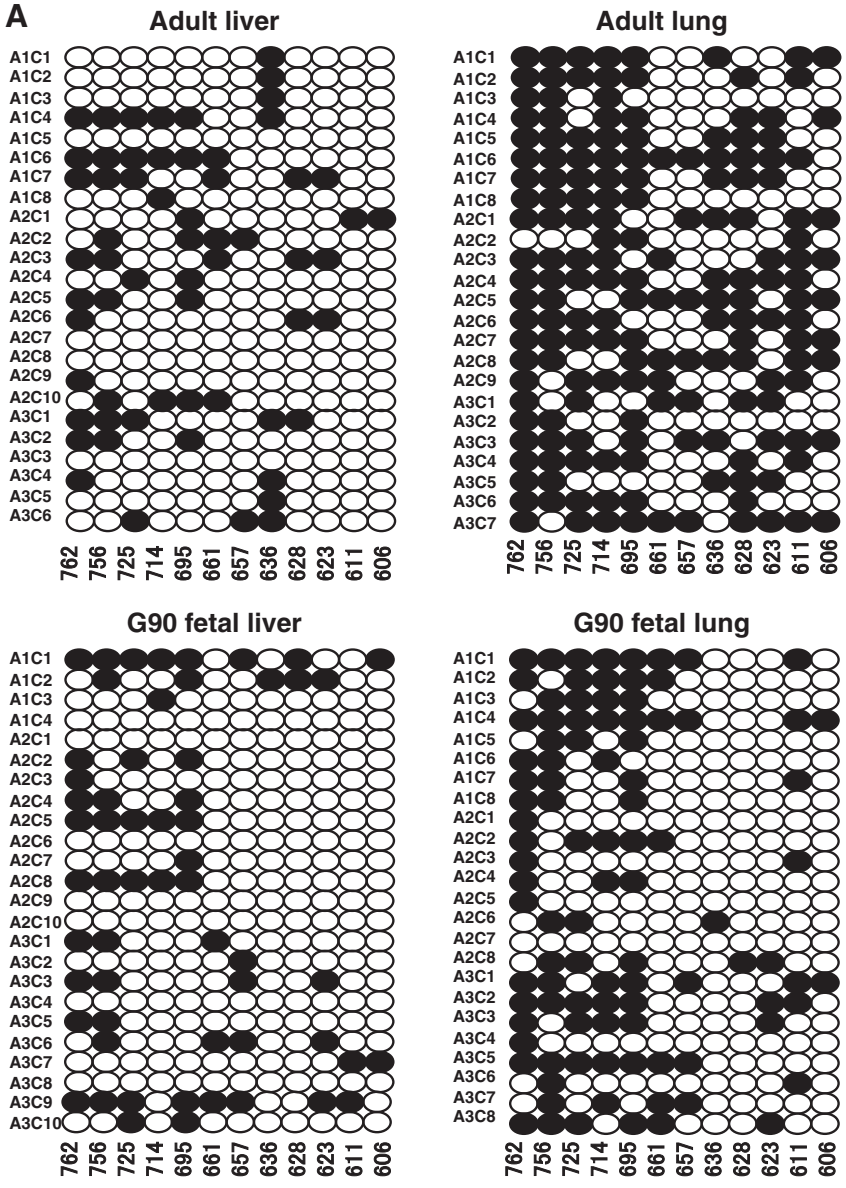

Fig. 4. CpG island consisting of 72 CpG sites of *bhmt* gene was amplified in four overlapping regions for adult liver, adult lung, G90 liver and G90lungs. The primer set Mp-1 was used to amplify region 1(A), primer set Mp-2 for region 2(B), primer set Mp-3 for region 3(C) and primer set Mp-4 for region 4(D). For each primer set a total of 24 clones (exception 23 clones were obtained for G90 liver, primer set Mp-3) were isolated. The number of clones (C) obtained from each animal (A) is indicated in the figure. A minimum of four clones from each of the three animals for each primer set was sequenced. The open circles indicate unmethylated CpG sites whereas black circles indicate methylated CpG sites. The black boxes indicate the putative transcriptional binding sites. The negative numbering denotes regions that are upstream of the transcription start site, whereas positive numbers indicate nucleotide sequence downstream of the transcription start site.

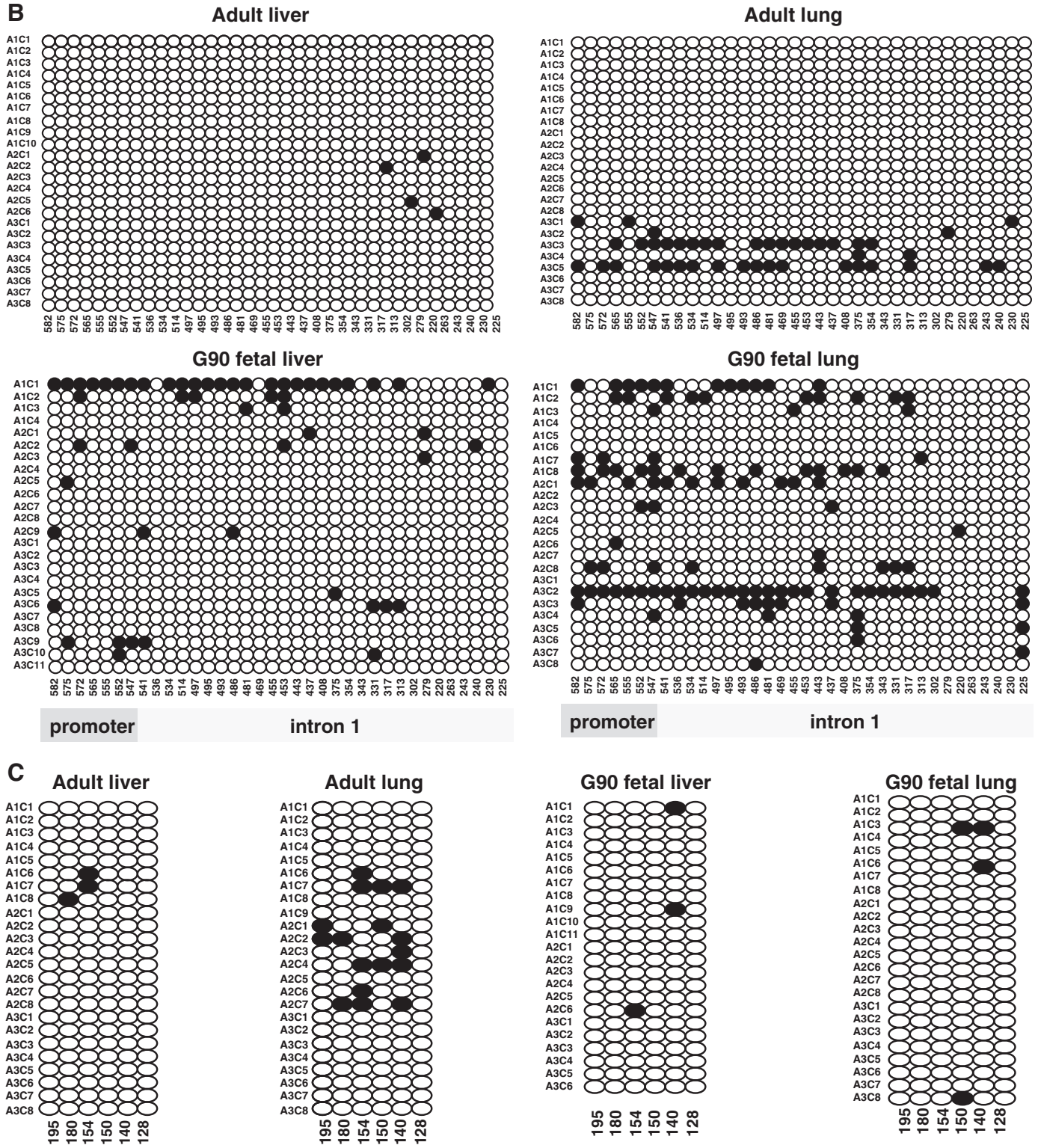

Fig. 4 (*continued*).

secondary structure of a leader sequence is stable (−50 kcal/mol) there can be an 85–95% reduction in the translation compared to transcripts with unstable secondary structures (Kozak, 1986). Numerous studies have shown that alternative splicing is one mechanism whereby a long and GC rich 5′ UTR that encodes a stable secondary structure can be truncated resulting in a reduction in the stability of the leader

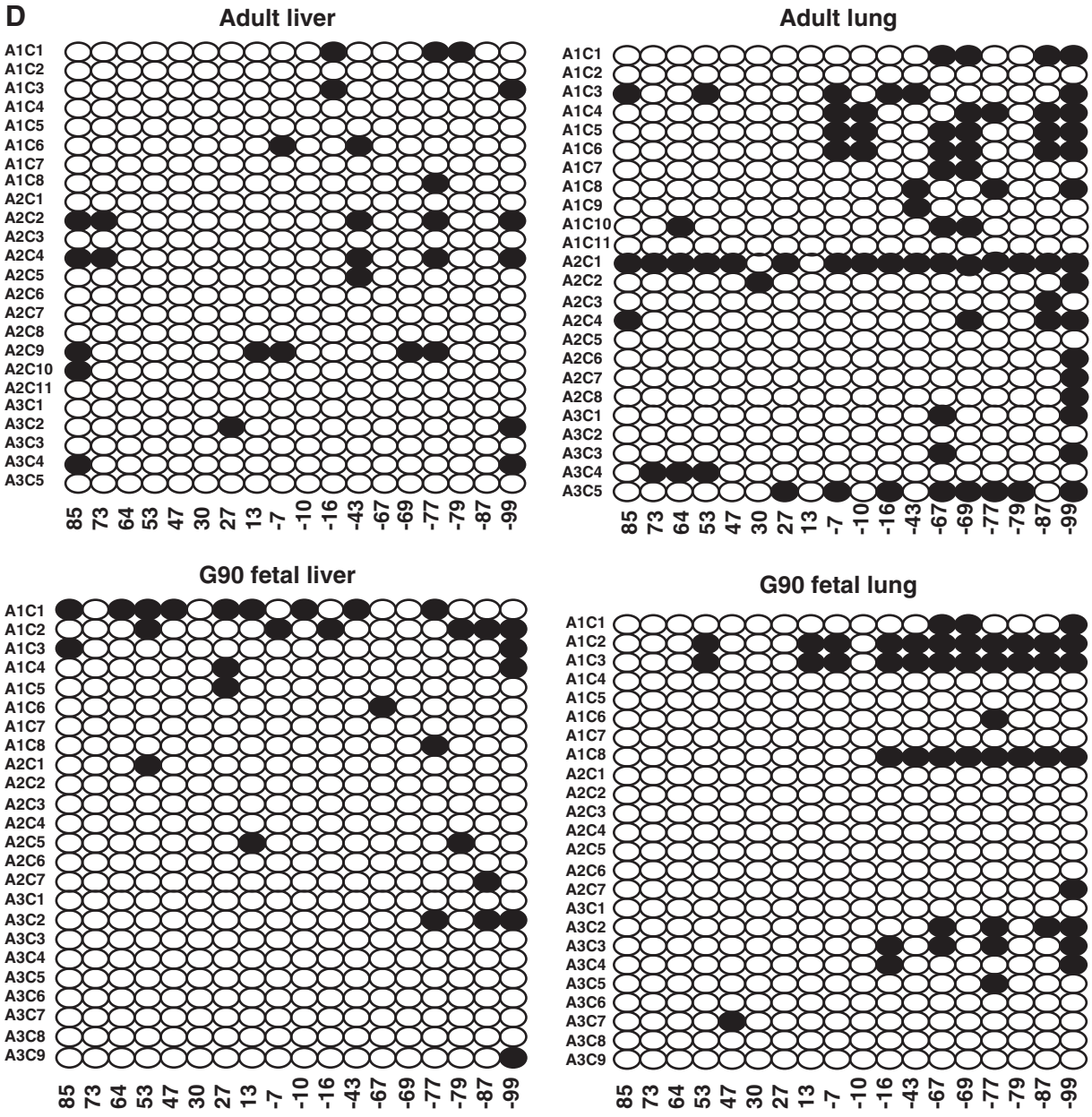

Fig. 4 (*continued*).

sequence's secondary structure and in turn enhance protein translation (Charron et al., 1998; Delgado-Reyes et al., 2001; Han et al., 2003; Sasahara et al., 1998). This phenomena appears to be occurring with respect to *bhmt* expression since the 162 bp leader sequence observed in the heart (SV5 and SV6, 61% GC content) was predictably more stable than the 77 bp leader sequence detected in the liver (SV1, 52% GC content). However, the 5′ UTR in brain (SV7) is only 3 bp shorter than the dominant liver isoform (SV1) and shares similar secondary structures and free energies, and yet brain, unlike liver, does not express significant levels of BHMT activity indicating other mechanisms besides 5′ UTR structure and stability inhibiting BHMT mRNA expression must be present in brain tissue. Overall, however, it is likely that the spatial and temporal differences in BHMT enzyme expression across tissues are in part due to factors associated with *bhmt* transcript variations within 5′ UTRs.

The 3′ UTRs of the *bhmt* transcripts also displayed considerable variation (Fig. 2, Table 2). It is interesting to note that those organs that expressed low or negligible levels of BHMT activity (kidney medulla, lungs, heart, brain) expressed transcripts with significantly shorter 3′ UTRs compared to the liver and kidney cortex, whose dominant variant (SV1) have the longest 3′ UTR, and highest levels of BHMT mRNA and activity.

In general, miRNA functions by degrading the transcript and/or translational repression (Bartel, 2009). Using miRNA predicting software, a potential miRNA binding site has been identified in murine *bhmt* 3′ UTR and this miRNA site is conserved in SV1 and SV8. These data suggest that the length of the 3′ UTR in the different *bhmt* SV affects transcript stability and subsequent level of protein expression (Gaidatzis et al., 2007; Majoros and Ohler, 2007; Thiele et al., 2006; Thorrez et al., 2010).

The expression of *bhmt* transcripts and BHMT activity was highest in adult pig liver and kidney cortex in accordance to previous findings (Delgado-Reyes et al., 2001; Ganu et al., 2011; Sunden et al., 1997). Even though *bhmt* transcripts were detected in kidney medulla, lungs,

heart and brain, negligible levels of enzyme activity were detected in these organs except for low levels in the brain. The *bhmt* transcripts and enzyme activity were developmentally regulated. There was a clear trend of increasing *bhmt* transcript expression and enzyme activity with age in the liver, and the magnitude of mRNA expression and enzyme activity in adult liver was approximately 100 times higher when compared to fetal liver. It is currently unknown what factors (dietary or environmental) stimulate BHMT expression following birth, or conversely, repress fetal expression.

The variants that encode tBHMT represented 5–13% of the total *bhmt* mRNA found in G30 fetuses, G45 liver, adult liver and kidney cortex. This suggests that tBHMT could be translated at significant levels in adult liver and kidney cortex, but we were unable to determine if it was present in these organs because our polyclonal antibodies against BHMT do not recognize a peptide smaller than 45 kD in crude pig liver or kidney extracts (Delgado-Reyes and Garrow, 2005). An *in silico* model of tBHMT suggests that this hypothetical protein would assume a horseshoe fold rather than the wild type $(\beta/\alpha)_8$ barrel characteristic of BHMT enzymes (Evans et al., 2002; Gonzalez et al., 2004). If expressed and stable, tBHMT would not be a Hcy methyltransferase since it lacks residues required for Zn binding, which prevents the protein's ability to bind Hcy (Breksa and Garrow, 2002; Castro et al., 2004; Evans et al., 2002). Generally, proteins that assume a horseshoe fold function as chaperones or inhibitors, for example ribonuclease inhibitor protein (Papageorgiou et al., 1997), and so it is possible that the tBHMT demonstrates chaperone or protein inhibitor functions. Recently a study demonstrated a *bhmt* splice variant in hepatic cancer that caused a frameshift in exon 4 resulting in a termination codon (Pellanda et al., 2012). This variant was not observed in healthy liver, and hence was not isolated by our study.

The methylation of DNA, RNA, and histone proteins are known to have significant affects on gene expression and phenotype (Niemitz and Feinberg, 2004; Wolff et al., 1998; Xin et al., 2003). Specifically methylation of CpG islands generally within the promoter and/or overlap critical transcription factor binding sites decreases gene transcription when they were found. Both these factors seem to affect the spatial expression of the *BHMT* gene. The methylation status of the *BHMT* gene in adult liver was five times lower than observed in adult lungs, and the latter organ expresses significantly lower levels of *bhmt* mRNA. Recently, a study demonstrated that global DNA hypomethylation in fetal brain was correlated to neural tube defect-associated pregnancy (Chen et al., 2010). Hyperhomocysteinemia has been associated with neural tube defects and loss of BHMT function causes hyperhomocysteinemia. Therefore it would be interesting to determine if BHMT is expressed in the neural tube and if methylation status of the *bhmt* gene is associated with neural tube closure.

In summary, the results reported herein indicate that many organs express different variants of *bhmt*, and that by far the highest levels of BHMT mRNA in pigs was observed in the liver and kidney cortex. The discovery of *bhmt* splice variants that differ in their 5′ and 3′ UTRs, in combination with the variation observed in the methylation status of the *BHMT* gene in different organs are likely factors affecting the organ distribution of BHMT activity.

Conflict of interest

The authors declare no conflict of interest.

Acknowledgments

This work was supported by USDA AG 2008-34480-19328 and USDA-ARS 538 AG58-5438-7-317l to LBS, and NIH grant RO1 DK52501 to TAG. The funding agencies were not involved in the preparation of the manuscript. We thank the staff at W.M. Keck Center for Comparative and Functional Genomics at UIUC for their help in sequencing and real-time RT-PCR.

References

Refsum, H., Ueland, P.M., Nygard, O., Vollset, S.E., 1998. Homocysteine and cardiovascular disease. Annu. Rev. Med. 49, 31–62.
Ananth, C.V., et al., 2007. Polymorphisms in methionine synthase reductase and betaine–homocysteine S-methyltransferase genes: risk of placental abruption. Mol. Genet. Metab. 91, 104–110.
Eskes, T.K., 1998. Neural tube defects, vitamins and homocysteine. Eur. J. Pediatr. 157 (Suppl. 2), S139–S141.
Hague, W.M., 2003. Homocysteine and pregnancy. Best Pract. Res. Clin. Obstet. Gynaecol. 17, 459–469.
James, S.J., et al., 1999. Abnormal folate metabolism and mutation in the methylenetetrahydrofolate reductase gene may be maternal risk factors for Down syndrome. Am. J. Clin. Nutr. 70, 495–501.
Mills, J.L., et al., 1995. Homocysteine metabolism in pregnancies complicated by neural-tube defects. Lancet 345, 149–151.
Steegers-Theunissen, R.P., Boers, G.H., Trijbels, F.J., Eskes, T.K., 1991. Neural-tube defects and derangement of homocysteine metabolism. N. Engl. J. Med. 324, 199–200.
Petrossian, T.C., Clarke, S.G., 2011. Uncovering the human methyltransferasome. Mol. Cell. Proteomics 10 (M110 000976).
Szegedi, S.S., Castro, C.C., Koutmos, M., Garrow, T.A., 2008. Betaine–homocysteine S-methyltransferase-2 is an S-methylmethionine-homocysteine methyltransferase. J. Biol. Chem. 283, 8939–8945.
Garrow, T.A., 1996. Purification, kinetic properties, and cDNA cloning of mammalian betaine–homocysteine methyltransferase. J. Biol. Chem. 271, 22831–22838.
Millian, N.S., Garrow, T.A., 1998. Human betaine–homocysteine methyltransferase is a zinc metalloenzyme. Arch. Biochem. Biophys. 356, 93–98.
Evans, J.C., et al., 2002. Betaine–homocysteine methyltransferase: zinc in a distorted barrel. Structure 10, 1159–1171.
Gonzalez, B., Pajares, M.A., Martinez-Ripoll, M., Blundell, T.L., Sanz-Aparicio, J., 2004. Crystal structure of rat liver betaine homocysteine s-methyltransferase reveals new oligomerization features and conformational changes upon substrate binding. J. Mol. Biol. 338, 771–782.
Delgado-Reyes, C.V., Garrow, T.A., 2005. High sodium chloride intake decreases betaine–homocysteine S-methyltransferase expression in guinea pig liver and kidney. Am. J. Physiol. Regul. Integr. Comp. Physiol. 288, R182–R187.
Tumbleson, M.E., Schook, L.B. (Eds.), 1996. Advances in Swine in Biomedical Research, vol. 1-2. Plenum Press, New York.
Sunden, S.L., Renduchintala, M.S., Park, E.I., Miklasz, S.D., Garrow, T.A., 1997. Betaine–homocysteine methyltransferase expression in porcine and human tissues and chromosomal localization of the human gene. Arch. Biochem. Biophys. 345, 171–174.
Johnson, J.M., et al., 2003. Genome-wide survey of human alternative pre-mRNA splicing with exon junction microarrays. Science 302, 2141–2144.
Ganu, R.S., Garrow, T.A., Sodhi, M., Rund, L.A., Schook, L.B., 2011. Molecular characterization and analysis of the porcine betaine homocysteine methyltransferase and betaine homocysteine methyltransferase-2 genes. Gene 473, 133–138.
Zuker, M., 2003. Mfold web server for nucleic acid folding and hybridization prediction. Nucleic Acids Res. 31, 3406–3415.
Chen, K., Rund, L.A., Beever, J.E., Schook, L.B., 2006. Isolation and molecular characterization of the porcine transforming growth factor beta type I receptor (TGFBR1) gene. Gene 384, 62–72.
Breksa III, A.P., Garrow, T.A., 2002. Random mutagenesis of the zinc-binding motif of betaine–homocysteine methyltransferase reveals that Gly 214 is essential. Arch. Biochem. Biophys. 399, 73–80.
Kelley, L.A., Sternberg, M.J.E., 2009. Protein structure prediction on the web: a case study using the Phyre server. Nat. Protoc. 4, 363–371.
Schrodinger, L.L.C., 2010. The PyMOL Molecular Graphics System, Version 1.3r1.
Kozak, M., 1986. Influences of mRNA secondary structure on initiation by eukaryotic ribosomes. Proc. Natl. Acad. Sci. U. S. A. 83, 2850–2854.
Charron, M., Shaper, J.H., Shaper, N.L., 1998. The increased level of beta1,4-galactosyltransferase required for lactose biosynthesis is achieved in part by translational control. Proc. Natl. Acad. Sci. U. S. A. 95, 14805–14810.
Delgado-Reyes, C.V., Wallig, M.A., Garrow, T.A., 2001. Immunohistochemical detection of betaine–homocysteine S-methyltransferase in human, pig, and rat liver and kidney. Arch. Biochem. Biophys. 393, 184–186.
Han, B., Dong, Z., Zhang, J.T., Han, B., Dong, Z., Zhang, J.T., 2003. Tight control of platelet-derived growth factor B/c-sis expression by interplay between the 5′-untranslated region sequence and the major upstream promoter. J. Biol. Chem. 278, 46983–46993.
Sasahara, M., et al., 1998. Normal developing rat brain expresses a platelet-derived growth factor B chain (c-sis) mRNA truncated at the 5′ end. Oncogene 16, 1571–1578.
Bartel, D.P., 2009. MicroRNAs: target recognition and regulatory functions. Cell 136 (2, 23), 215–233.
Gaidatzis, D., van Nimwegen, E., Hausser, J., Zavolan, M., 2007. Inference of miRNA targets using evolutionary conservation and pathway analysis. BMC Bioinforma. 8, 69.
Majoros, W.H., Ohler, U., 2007. Spatial preferences of microRNA targets in 3′ untranslated regions. BMC Genomics 8, 152.
Thiele, A., Nagamine, Y., Hauschildt, S., Clevers, H., 2006. AU-rich elements and alternative splicing in the beta-catenin 3′UTR can influence the human beta-catenin mRNA stability. Exp. Cell Res. 312, 2367–2378.
Thorrez, L., Tranchevent, L.C., Chang, H.J., Moreau, Y., Schuit, F., 2010. Detection of novel 3′ untranslated region extensions with 3′ expression microarrays. BMC Genomics 11, 205.
Castro, C., et al., 2004. Dissecting the catalytic mechanism of betaine–homocysteine S-methyltransferase by use of intrinsic tryptophan fluorescence and site-directed mutagenesis. Biochemistry 43, 5341–5351.

Papageorgiou, A.C., Shapiro, R., Acharya, K.R., 1997. Molecular recognition of human angiogenin by placental ribonuclease inhibitor—an X-ray crystallographic study at 2.0 A resolution. EMBO J. 16, 5162–5177.
Pellanda, H., et al., 2012. A splicing variant leads to complete loss of function of betaine–homocysteine methyltransferase (BHMT) gene in hepatocellular carcinoma. Int. J. Biochem. Cell Biol. 44, 385–392.
Niemitz, E.L., Feinberg, A.P., 2004. Epigenetics and assisted reproductive technology: a call for investigation. Am. J. Hum. Genet. 74, 599–609.
Wolff, G.L., Kodell, R.L., Moore, S.R., Cooney, C.A., 1998. Maternal epigenetics and methyl supplements affect agouti gene expression in Avy/a mice. FASEB J. 12, 949–957.
Xin, Z., Tachibana, M., Guggiari, M., Heard, E., Shinkai, Y., Wagstaff, J., 2003. Role of histone methyltransferase G9a in CpG methylation of the Prader–Willi syndrome imprinting center. J. Biol. Chem. 278, 14996–15000.
Chen, X., et al., 2010. Global DNA hypomethylation is associated with NTD-affected pregnancy: a case–control study. Birth Defects Res. A Clin. Mol. Teratol. 88, 575–581.